STRICT SUBGOAL EXECUTION: RELIABLE LONG-HORIZON PLANNING IN HIERARCHICAL REINFORCEMENT LEARNING

Anonymous authors
Paper under double-blind review

ABSTRACT

Long-horizon goal-conditioned tasks pose fundamental challenges for reinforcement learning (RL), particularly when goals are distant and rewards are sparse. While hierarchical and graph-based methods offer partial solutions, their reliance on conventional hindsight relabeling often fails to correct subgoal infeasibility, leading to inefficient high-level planning. To address this, we propose Strict Subgoal Execution (SSE), a graph-based hierarchical RL framework that integrates Frontier Experience Replay (FER) to separate unreachable from admissible subgoals and streamline high-level decision making. FER delineates the reachability frontier using failure and partial-success transitions, which identifies unreliable subgoals, increases subgoal reliability, and reduces unnecessary high-level decisions. Additionally, SSE employs a decoupled exploration policy to cover underexplored regions of the goal space and a path refinement that adjusts edge costs using observed low-level failures. Experimental results across diverse long-horizon benchmarks show that SSE consistently outperforms existing goal-conditioned and hierarchical RL methods in both efficiency and success rate.

1 INTRODUCTION

Recent advances in reinforcement learning (RL) have achieved impressive success across various domains (Mnih et al., 2013; Silver et al., 2016). In many real-world applications, agents must achieve specific objectives, motivating the development of goal-conditioned RL (GCRL), where agents learn to reach a designated goal state provided by the environment (Schaul et al., 2015; Levy et al., 2017; Nasiriany et al., 2019). Unlike conventional RL methods that rely on carefully designed reward functions, GCRL allows agents to directly pursue target states based on goal specifications. However, in sparse-reward and long-horizon environments, goals are often distant, making exploration difficult and hindering effective learning due to a lack of intermediate guidance.

To address this, hierarchical RL (HRL) decomposes the decision process into a high-level policy that selects subgoals and a low-level policy that executes actions to reach them (Bacon et al., 2017; Vezhnevets et al., 2017). Since subgoals are typically closer and more attainable than the final goal, this structure facilitates learning in long-horizon settings. Nevertheless, HRL can still fail when the selected subgoals are too difficult for the low-level policy to reach reliably. To mitigate this issue, graph-based HRL methods have been proposed (Zhang et al., 2018; Nachum et al., 2018a; Huang et al., 2019; Eysenbach et al., 2019; Kim et al., 2021; Zhang et al., 2021). These approaches construct a graph over the goal space, where nodes represent states or regions and edges denote feasible transitions. Subgoal selection is guided by shortest paths on the graph, improving success rates in complex tasks. However, even graph-based HRL remains limited in performance when the final goal lies far from the current state, as the high-level policy may require too many steps, resulting in unstable training and poor scalability.

While recent approaches have explored graph-based GCRL without hierarchical structures to mitigate the limitations of high-level policies, such methods often lack the flexibility to handle environments involving multiple goals or diverse reward signals because they omit high-level reasoning (Lee et al., 2023; Yoon et al., 2024). To address these limitations, we propose a graph-based HRL framework, **Strict Subgoal Execution (SSE)**, which retains the advantages of high-level planning and

improves long-horizon goal reaching by combining a new replay scheme with targeted exploration and path refinement. Our contributions are summarized as follows:

1. **Frontier Experience Replay (FER) for SSE:** We introduce FER, which delineates the reachability frontier using two high-level samples: failure transitions and partial-success transitions. By precisely localizing where attempts fail and how far progress extends, FER identifies unreliable subgoals, increases subgoal reliability and reduces unnecessary high-level decisions.
2. **Decoupled Exploration for Goal Space Coverage:** A dedicated exploration policy is decoupled from the return-driven high-level policy to traverse underexplored regions of the goal space, improving coverage and sample efficiency.
3. **Failure-Aware Path Refinement:** To improve subgoal reliability, we adjust graph edge costs based on low-level failure statistics, encouraging path planning to avoid unstable transitions and strengthening subgoal execution.

Through extensive evaluation on diverse long-horizon, goal-conditioned tasks, our method demonstrates higher success rates and better sample efficiency than prior GCRL and HRL approaches, validating the effectiveness of the proposed SSE framework.

2 PRELIMINARIES

2.1 UNIVERSAL MDP, GOAL-CONDITIONED RL, AND GOAL RELABELING TECHNIQUES

We consider a universal Markov decision process (UMDP) defined as a tuple $(\mathcal{S}, \mathcal{G}, \mathcal{A}, P, R, \gamma)$, where $\mathcal{S}$ is the state space, $\mathcal{G}$ is the goal space, $\mathcal{A}$ is the action space, P is the transition dynamics, R is the reward function, and $\gamma \in (0, 1]$ is the discount factor (Schaul et al., 2015). At each time step t, the agent observes a goal $g \in \mathcal{G}$ and state s_t, selects an action $a_t \sim \pi(\cdot|s_t, g)$, and receives a reward $r_t = R(s_t, a_t, s_{t+1}, g)$ and next state $s_{t+1} \sim P(\cdot|s_t, a_t)$. The goal of GCRL is to learn a goal-conditioned policy π that maximizes the expected return $\sum_{t=0}^{H} r_t$, where H is the episode length. When $\mathcal{S} \neq \mathcal{G}$, we assume the existence of a mapping ϕ such that $\phi(s) \in \mathcal{G}$, allowing the agent to infer goal progress from the current state. The goal g can be either fixed or randomly sampled in each episode. In long-horizon goal-conditioned settings, learning is often inefficient due to the lack of positive signals. To mitigate this, goal relabeling techniques such as Hindsight Experience Replay (HER) (Andrychowicz et al., 2017) treat states achieved later in a trajectory as substitute goals and can be applied to improve sample efficiency. HER augments the replay by replacing the intended goal g with a future achieved goal $g' = \phi(s_{t'})$ for some $t' \geq t$ and recomputing the reward:

$$(s_t, a_t, r_t, s_{t+1}, g) \;\mapsto\; (s_t, a_t, R(s_t, a_t, s_{t+1}, g'), s_{t+1}, g').$$

This converts unsuccessful attempts into useful signals while the original transitions unchanged.

2.2 HRL FRAMEWORKS AND GRAPH-BASED SUBGOAL PLANNING IN GCRL

In goal-conditioned settings, HRL addresses long-horizon challenges by decomposing the policy into a high-level policy π^h and a low-level policy π^l (Bacon et al., 2017; Vezhnevets et al., 2017). Every k steps, $\pi^h(\cdot \mid s_t, g)$ selects a subgoal $\tilde{g}_t \in \mathcal{G}$, which $\pi^l(\cdot \mid s_t, \tilde{g}_t)$ attempts to reach using an auxiliary reward (Zhang et al., 2020; Pateria et al., 2021; Hutsebaut-Buysse et al., 2022). However, when subgoals are too distant, the low-level policy may fail to reach them within the given horizon, and distance-based penalties can hinder learning under sparse rewards. To mitigate this, graph-based approaches construct a goal-space graph $G = (V, E)$, where V is a set of landmark nodes and E contains edges weighted by the effort to transition between nodes. Landmarks are commonly chosen via farthest point sampling (FPS) (Kim et al., 2021; Lee et al., 2022; Park et al., 2024) or placed on a predefined grid over the goal space (Yoon et al., 2024), assuming that the goal space is known to define the graph and the high-level policy. In general, the edge cost is defined as

$$d(v_1 \to v_2) := \log_\gamma(1 + (1 - \gamma)Q^G(v_1, v_2, \pi^l)), \tag{1}$$

where Q^G estimates the feasibility of reaching v_2 from v_1 under π^l, defined as the value function Q^l of the low-level policy or a predefined estimator. Full details on Q^G are provided in Appendix B.1. In graph-based HRL, given a subgoal $\tilde{g}_t$, the shortest path from the current state's embedding $\phi(s_t)$

to $\tilde{g}_t$ is computed via Dijkstra's algorithm (Dijkstra, 1959), producing a sequence of waypoints $(\mathrm{wp}_1, \ldots, \mathrm{wp}_n)$, where each $\mathrm{wp}_i \in V$. The low-level policy $\pi^l(\cdot|s_t, \mathrm{wp}_i)$ guides the agent through these waypoints in order: once wp_i is reached, the next target for π^l is updated to wp_{i+1}, continuing until $\tilde{g}_t$ is reached. The high-level policy is trained on transitions $(s_t, g, \tilde{g}_t, \sum_{j=t}^{t+k-1} r_j, s_{t+k})$ in buffer $\mathcal{B}_F^h$, while the low-level policy π^l is trained using $(s_t, \mathrm{wp}_i, a_t, r_t^l, s_{t+1})$ in buffer $\mathcal{B}^l$, where the low-level reward $r_t^l = -1$ if the agent has not reached wp_i, and $r_t^l = 0$ otherwise (Kim et al., 2021; Lee et al., 2022; Park et al., 2024). In contrast, certain approaches dispense with high-level subgoals and directly train the low-level policy to reach the final goal g, under the assumption that intermediate subgoals are unnecessary (Lee et al., 2023; Yoon et al., 2024).

3 Related work

Goal-Conditioned RL and Hierarchical Approaches GCRL refers to RL settings where the agent is explicitly conditioned on a goal (Kaelbling, 1993; Liu et al., 2022; Colas et al., 2022). Modern GCRL typically employs Universal Value Function Approximators (UVFA) (Schaul et al., 2015) to generalize across goals. A central challenge is solving long-horizon tasks with sparse rewards, where exploration is difficult. To address this, HRL introduces multi-level policies that decompose complex tasks into temporally abstract subgoals (Vezhnevets et al., 2017), and the effectiveness of this decomposition has been demonstrated in diverse settings (Barto & Mahadevan, 2003; Kulkarni et al., 2016; Nachum et al., 2018a; 2019). Beyond hierarchical structures, other methods improve sample efficiency through structured exploration, such as prioritizing novel states (Warde-Farley et al., 2018; Pong et al., 2019) or discovering useful goals via unsupervised learning (Mendonca et al., 2021; Ecoffet et al., 2021; Chane-Sane et al., 2021).

Graph-based Approaches in GCRL Graph-based approaches have been introduced to GCRL to provide a structured representation of the goal space, enabling planning over discrete landmarks and improving navigation in sparse-reward environments (Huang et al., 2019; Eysenbach et al., 2019; Kim et al., 2021). Early work used graph structures to represent the state space and to guide exploration (Zhang et al., 2018; Nachum et al., 2018a), and this direction has since evolved through integration with latent modeling (Zhang et al., 2021) and policy-driven graph construction (Kim et al., 2023). More recent advances focus either on aligning high-level decisions with low-level execution via graph-based planning (Lee et al., 2022) or on enhancing exploration with strategies such as frontier-based expansion (Park et al., 2024), curriculum-based goal selection (Lee et al., 2023), and virtual subgoal generation for broader coverage (Yoon et al., 2024).

Relabeling and Guidance Techniques in GCRL In sparse-reward GCRL, data relabeling is central for improving sample efficiency. HER converts failed trajectories into successes by replacing the intended goal with a future achieved goal (Andrychowicz et al., 2017). Since uniform hindsight-goal sampling can be suboptimal, subsequent work explores curriculum-based relabeling (Fang et al., 2019), novelty- or priority-driven goal sampling (Zeng et al., 2023), and hierarchical relabeling that better matches low-level behavior (Nachum et al., 2018b). Orthogonal guidance approaches discourage infeasible subgoals, for example via learned adjacency constraints (Zhang et al., 2020) or adversarially generated goals that are challenging yet achievable (Levy et al., 2017).

4 Methods

4.1 Motivation: Rethinking Subgoal Execution in Graph-Based HRL

In GCRL, many methods improve goal-reaching performance by adopting hindsight relabeling techniques such as HER (Andrychowicz et al., 2017), which treat intermediate states as virtual goals to provide additional training signals. Recent graph-based HRL methods typically apply this idea to both the low level and the high level. While this benefits the low level, it introduces a critical issue at the high level. Fig. 1(a) illustrates how graph-based HRL with HER operates: the high-level policy selects a subgoal $\tilde{g}_t$ given the current state s_t, and the low-level policy follows a waypoint path to reach it. If $\tilde{g}_t$ is unreachable due to limited skill, obstacles, or excessive distance, the agent stops at an intermediate state, and such subgoals should be avoided. When HER is applied, every visited state along the failed trajectory is treated as if it were the intended subgoal. This causes the high-level

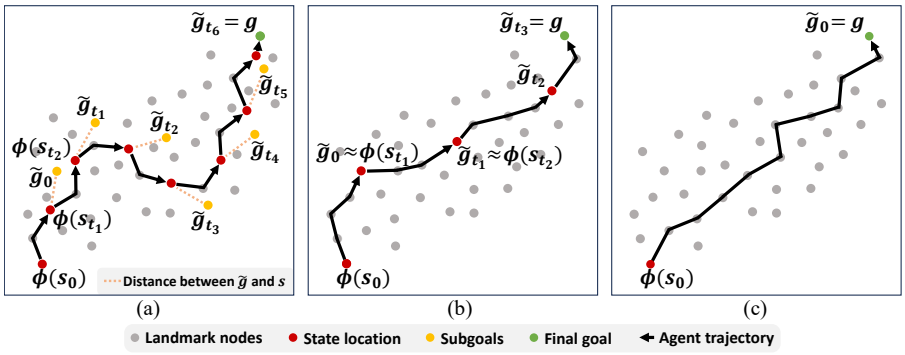

Figure 1: Agent trajectories in goal space $\mathcal{G}$. (a) Conventional HRL with HER relabels intermediate states as subgoals without enforcing exact subgoal completion, which lengthens high-level trajectories. (b) SSE with FER enforces exact subgoal completion, increasing subgoal reliability and reducing unnecessary high-level decisions, thereby improving learning efficiency. (c) After training, SSE reaches g with few high-level steps, here in a single step in single-goal settings even from distant starts. Agent locations are $\phi(s_t) \in \mathcal{G}$ and t_i is the i-th high-level step.

policy to repeatedly select ineffective subgoals and to waste many decision steps. In addition, the resulting transitions can vary widely for the same subgoal, which hinders stable learning. As shown in Fig. 1(a), this produces unnecessarily long high-level trajectories, and even if the agent reaches the goal g, credit is spread over too many steps, preventing earlier decisions from being reinforced and often leading to failure on long-horizon tasks.

To address this issue, we propose the Strict Subgoal Execution (SSE) framework, which updates the high-level policy with positive returns only when the low level successfully reaches the assigned subgoal. We instantiate this principle with Frontier Experience Replay (FER). Unlike relabeling methods such as HER that synthesize additional successes, FER delineates the reachability frontier by recording two types of high-level samples, failure transitions and partial-success transitions. By precisely localizing where attempts fail and how far progress extends, FER identifies unreliable subgoals, provides consistent training signals, and reduces unnecessary high-level decisions. As shown in Fig. 1(b), this separation of success and failure keeps the resulting state $\phi(s_{t'})$ closely aligned with the selected subgoal $\tilde{g}_t$, producing consistent high-level transitions and eliminating wasteful actions. Consequently, as illustrated in Fig. 1(c), the resulting high-level policy solves tasks with far fewer decisions, often reaching the final goal g in a single step in simple settings and handling multi-goal or long-horizon environments with only a few well-chosen subgoal selections.

4.2 Strict Subgoal Execution with Frontier Experience Replay

In this section, we describe the details of the SSE framework. We first define FER, the key component of SSE, which marks the reachability frontier by recording two high-level sample types in addition to standard successes: failure transitions that stop at the point of failure and partial-success transitions that record the last reliably reached waypoint. To formalize this, we basically follow the HRL setup from Section 2: At each time t, the policy selects a subgoal $\tilde{g}_t \in \mathcal{G}$ under the common assumption that the goal space $\mathcal{G}$ is known. A waypoint path $(\mathrm{wp}_1, \ldots, \mathrm{wp}_n)$ on the graph $G = (V, E)$ is then generated, and the low-level policy π^l follows this path until termination at time t'. We regard the subgoal as reachable if $\|\phi(s_{t'}) - \tilde{g}_t\| < \lambda$; otherwise the attempt is treated as a failure. In the failure case, $\mathrm{wp}_{\mathrm{final}}$ denotes the last waypoint reached within tolerance before failure. Based on this notion of reachability, we define FER as follows.

Definition 4.1 (Frontier Experience Replay) *The high-level replay buffer $\mathcal{B}_F^h$ stores transitions as*

$$\mathcal{B}_F^h = \begin{cases} (s_t, g, \tilde{g}_t, \sum_{j=t}^{t'-1} r_j, s_{t'}) \textit{ (success)} & \textit{if } \|\phi(s_{t'}) - \tilde{g}_t\| < \lambda, \\ (s_t, g, \tilde{g}_t, 0, s_T) \textit{ (stop-on-failure)} & \textit{if } \|\phi(s_{t'}) - \tilde{g}_t\| \geq \lambda, \\ (s_t, g, \mathrm{wp}_{\mathrm{final}}, \sum_{j=t}^{t_{\mathrm{wp}}-1} r_j, s_{t_{\mathrm{wp}}}) \textit{ (partial success)} & \textit{if failure occurs and } \mathrm{wp}_{\mathrm{final}} \textit{ exists}. \end{cases} \tag{2}$$

Here, s_T is the terminal state, $\sum_j r_j$ is the cumulative reward collected until reaching the subgoal or waypoint, and t_{wp} is the time step at which $\mathrm{wp}_{\mathrm{final}}$ is reached.

In FER, *a success transition* records the full cumulative return up to t' and continues the episode, *a stop-on-failure transition* assigns zero return and sets the next state to s_T, which immediately truncates the episode so all future returns are forfeited and unreachable or unreliable subgoals are discouraged, and *a partial-success transition* records $\mathrm{wp}_{\mathrm{final}}$ with its accumulated return, localizing how far the attempt progressed and crediting only the reliably executed portion. Together, these signals delineate the reachability frontier, identify unreliable subgoals, and provide consistent high-level targets that reduce unnecessary high-level decisions. This setup separates reliable from unreliable subgoals and suppresses failure-inducing actions, but it can induce conservatism and reduce exploratory coverage because the agent learns to avoid regions associated with failure. To counterbalance this effect, we introduce a decoupled high-level controller comprising a high-level policy π^h for exploitation trained on $\mathcal{B}_F^h$ and a complementary exploration policy $\pi^{\exp}$ that promotes coverage. As in prior graph-based HRL, we assume the goal space $\mathcal{G}$ is known for subgoal selection of both π^h and $\pi^{\exp}$, and SSE introduces no additional assumptions. Detailed formulations follow.

High-level Policy π^h: In prior work, subgoals are typically selected with Gaussian policies with small noise. Although adequate for those methods, this concentrates exploration near the current maximum subgoal. As noted above, we aim for a high-level policy that can target any point in the goal space, thereby broadening exploration. We therefore define an ϵ-greedy π^h as

$$\pi^h(\tilde{g}_t \mid s_t, g) = \begin{cases} \tilde{g}_{\max,t} := \arg\max_{\tilde{g}\in\mathcal{G}} Q^h(s_t, \tilde{g}, g) & \text{with probability } 1-\epsilon, \\ \tilde{g}_{\mathrm{rand}} \sim \mathrm{Uniform}(\mathcal{G}) & \text{with probability } \epsilon, \end{cases} \tag{3}$$

where $\tilde{g}_{\max,t}$ is the greedy subgoal, in practice generated by the actor network trained to choose the maximum of Q^h, $\tilde{g}_{\mathrm{rand}}$ is sampled uniformly from $\mathcal{G}$ to ensure persistent global exploration, and Q^h is trained off-policy using $\mathcal{B}_F^h$. This formulation allows π^h to select diverse points in the goal space independently of the agent's current location, which is crucial for broader exploration.

Exploration Policy $\pi^{\exp}$: To promote exploration, $\pi^{\exp}$ targets low-density, underexplored regions of the goal space. In the 2D and 3D goal space settings considered here, we indentify the novel regions with a grid-based estimator for simplicity and computational efficiency. The component is modular and can be replaced by other density estimators in general higher-dimensional goal spaces, for example kernel density, k-NN counts, or learned novelty models, without changing key components, SSE or FER. Concretely, we partition $\mathcal{G}$ into cells $C_{\mathcal{G}}^m$ of size $d_{\mathcal{G}}$ and define $\pi^{\exp}$ as

$$\pi^{\exp}(\tilde{g}_t \mid s_t, g) = \begin{cases} g & \text{with probability } \frac{1}{3}, \\ \tilde{g}_{\max,t} & \text{with probability } \frac{1}{3}, \\ \tilde{g}_{\mathrm{novel}} \sim \mathrm{Uniform}(C_{\mathcal{G}}^{m_{\mathrm{novel}}}) & \text{with probability } \frac{1}{3}, \end{cases} \tag{4}$$

where $\tilde{g}_{\mathrm{novel}}$ is sampled from the least visited cell $C_{\mathcal{G}}^{m_{\mathrm{novel}}}$ with $m_{\mathrm{novel}} = \arg\min_m N(C_{\mathcal{G}}^m)$ determined by the visit count $N(C_{\mathcal{G}}^m)$. Both π^h and $\pi^{\exp}$ operate under the same SSE mechanism: episodes continue only upon successful subgoal completion and terminate on failure. To control exploration, we sample from $\pi^{\exp}$ early in training and then gradually mix it with π^h using a ratio $\eta : (1-\eta)$, where η controls exploration strength. This balanced scheme preserves coverage, accelerates the discovery of reachable subgoals, and improves high-level generalization.

To illustrate the behavior of the proposed method, Fig. 2 shows grid-wise visitation in the goal space and low-level trajectories toward various initial subgoals at three stages of training: (a) early (10K steps), (b) intermediate (150K steps), and (c) final (500K steps). The environment is a `U-maze` where a MuJoCo (Todorov et al., 2012) Ant agent navigates to the final goal g located at the upper left of the map. In (a), most of the goal space remains unexplored, and initial subgoals selected by $\pi^{\exp}$ and π^h, including the final goal, random subgoals, and novel regions, result in wide-ranging trajectories that promote broad exploration. As training progresses in (b), the agent expands its coverage across the map, and in (c), it consistently reaches the goal g. Notably, SSE enables the agent to reach any reachable subgoal in a single high-level step, regardless of distance, supporting reliable execution and efficient long-range planning. This allows the agent to solve complex tasks using only a few high-level decisions.

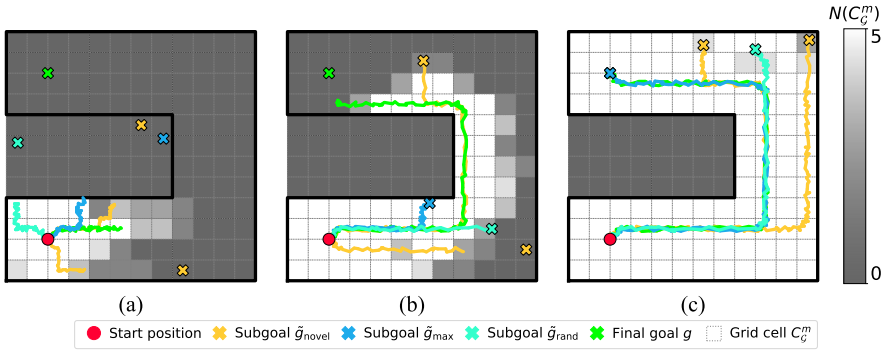

Figure 2: Initial subgoals at $t = 0$ selected by π^h and π^{exp}, with corresponding Ant agent trajectories at (a) early, (b) intermediate, and (c) final training stages in the U-maze task. The goal space (agent positions in the map) is partitioned into grid cells C_G^m. π^h selects between $\tilde{g}_{\text{max}}$ and $\tilde{g}_{\text{rand}}$ to encourage broad coverage, while π^{exp} samples from $\tilde{g}_{\text{novel}}$, $\tilde{g}_{\text{max}}$, and g to visit underexplored regions and the goal. Over time, unreachable areas are excluded from subgoal candidates via SSE.

4.3 Failure-Aware Path Refinement

In the SSE framework, reliable subgoal execution is crucial as each subgoal must be reached within a single high-level step. As described in Section 2, graph-based methods use Dijkstra's algorithm to compute waypoint paths from $\phi(s_t)$ to $\tilde{g}_t$ on a graph $G = (V, E)$, with edge distances defined by d in Eq. equation 1. However, this distance ignores failure cases like collisions or getting stuck, causing agents to fail even on the shortest path. We observe these failure-prone regions significantly hinder subgoal success. To address this, we introduce a *failure-aware path refinement* strategy that increases edge costs in unreliable regions, steering the planner toward safer alternatives. To implement this, we identify high-failure regions within the goal space, which is generally achieved via spatial density estimation of failed trajectories. For consistency with our exploration policy and to maintain computational efficiency in our domains, we leverage the same grid-based discretization. We define a cell's failure count, $N_{\text{fail}}(C_G^m)$, as the number of times an agent, targeting a subgoal outside the cell (i.e., $\tilde{g}_t \in C_G^{m'}, m' \neq m$), terminates the episode within it. This indicates a failure to exit the current region. To discourage this, we increase traversal costs by defining the failure ratio as $\text{ratio}_{\text{fail}}(C_G^m) = N_{\text{fail}}(C_G^m)/N(C_G^m)$, and refine the edge distance from node v_1 to v_2 as:

$$\tilde{d}(v_1 \to v_2) = d(v_1 \to v_2) \times \max\left(1, c_{\text{dist}} \cdot \text{ratio}_{\text{fail}}(C_G^m)\right), \quad \forall v_2 \in C_G^m, \quad \forall m, \tag{5}$$

where d is the original edge distance from Eq. equation 1, and $c_{\text{dist}} > 1$ is a scaling factor. To ensure low-level policy competence, a cell's failure count $N_{\text{fail}}(C_G^m)$ is activated only after λ_{count} successful visits. A higher failure ratio increases the adjusted distance, encouraging Dijkstra's algorithm to avoid unreliable regions.

Fig. 3 illustrates the effect of the proposed path refinement in a bottleneck environment. In (a), without refinement, the agent repeatedly follows the shortest path through a narrow corridor near a wall, often resulting in failure. In (b), with refinement applied, increased edge costs in high-failure regions steer Dijkstra's algorithm toward safer detours. When no alternatives exist (e.g., in the bottleneck), the agent still passes through, preserving reachability. This demonstrates that the refinement enhances subgoal success while maintaining overall reachability, supporting more stable execution in complex tasks. In summary, the proposed SSE framework is illustrated in Fig. 4, with a condensed version of the algorithm provided in Algorithm 1. The full algorithm and implementation details, including the graph construction and training losses, are provided in Appendix B.

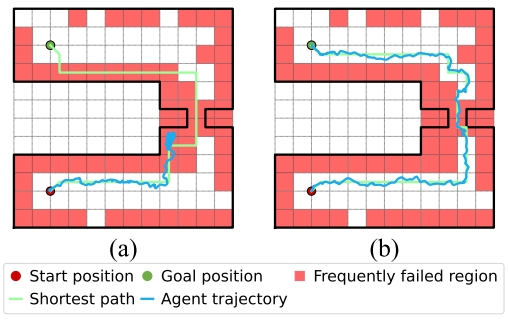

Figure 3: Comparison of agent trajectories (blue lines) in a map with a bottleneck: (a) without path refinement and (b) with the proposed path refinement. Green lines represent the shortest waypoint paths computed via Dijkstra's algorithm, while red areas denote grid cells with high failure ratios, i.e., $\text{ratio}_{\text{fail}}(C_G^m) > 0.05$.

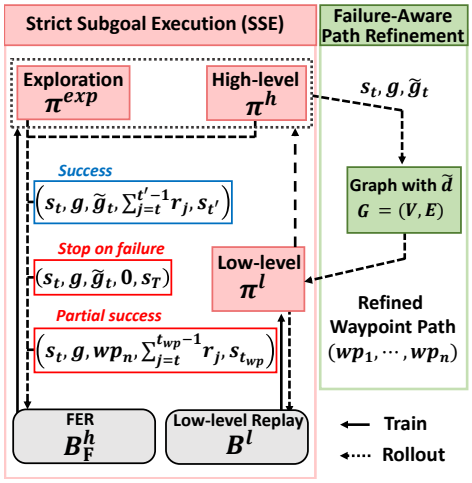

Figure 4: The proposed SSE framework.

Algorithm 1 Strict Subgoal Execution (SSE)

Initialize policies π^h, π^{exp}, π^l, and graph G
for *each iteration* **do**
  for *each episode* **do**
    for *each high-level selection step* **do**
      Sample a subgoal $\tilde{g}_t$ from π^h and π^{exp}
      Plan a waypoint path from $\phi(s_t)$ to $\tilde{g}_t$
      Roll out low-level policy $\pi^l(s_t, \text{wp}_i)\ \forall i$:
      if $\|\phi(s_{t'}) - \tilde{g}_t\| < \lambda$ *(success)* **then**
        Store the success transition and continue
      else
        Store the failure and partial-success transitions, then terminate the episode
      end
      $N_{\text{fail}}(C_{\mathcal{G}}^m) += 1$ if $\phi(s_{t'}) \in C_{\mathcal{G}}^m$
    end
    $N(C_{\mathcal{G}}^m) += 1$ for all visited grids $C_{\mathcal{G}}^m$
  end
  Update Q^h, Q^l, π^h, π^l via off-policy RL
end

5 Experiments

In this section, we evaluate our SSE framework on 9 challenging long-horizon tasks, including 5 AntMaze environments (`U-maze`, π`-maze`, `AntMazeComplex`, `AntMazeBottleneck`, and `AntMazeDoubleBottleneck`). These range from simple layouts (`U-maze`) to complex structures with narrow corridors (`AntMazeBottleneck`). We also assess 2 KeyChest tasks (`AntKeyChest`, `AntDoubleKeyChest`), where the agent must collect 1 or 2 keys before reaching the final goal, even though the keys are not explicitly defined as goals. Additionally, we evaluate 2 Reacher tasks (`ReacherWall`, `ReacherWallDoubleGoal`), where a 3D robot must navigate obstacles to reach one or two goals. KeyChest and DoubleGoal tasks require intermediate objectives, making them ideal for testing high-level planning. See Fig. 5 for visualizations and Appendix C for details. While the main experiments focus on fixed-goal settings, additional comparisons for random-goal setups are included in Appendix D.1.

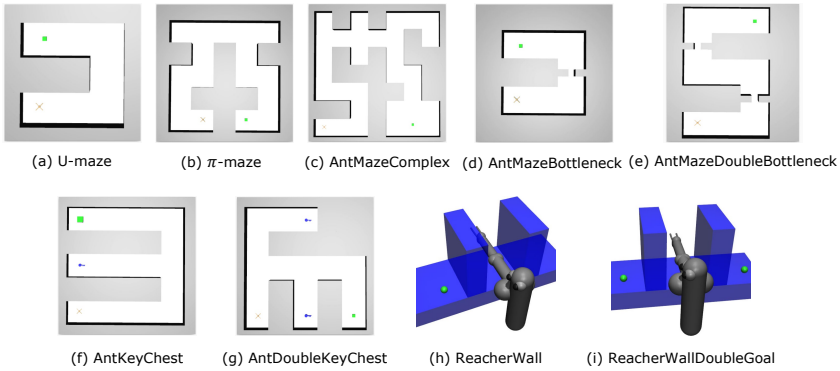

Figure 5: Considered long-horizon environments: 5 AntMaze, 2 KeyChest, and 2 Reacher tasks

5.1 Performance Comparison

We compare SSE with a range of hierarchical RL and recent graph-based methods. Specifically, we evaluate 2 HRL approaches: **HIRO** (Nachum et al., 2018b), which improves sample efficiency via hindsight goal relabeling, and **HRAC** (Zhang et al., 2020), which penalizes subgoal selection based on reachability. We also include 3 graph-based HRL methods: **HIGL** (Kim et al., 2021), which applies intrinsic penalties over a graph, **DHRL** (Lee et al., 2022), which finds a path and gives waypoints to low-level as a goal via graph palnning, and **NGTE** (Park et al., 2024), which expands graphs using novelty to better address fixed-goal settings. Additionally, we consider 2 graph-based methods without explicit high-level policies: **PIG** (Kim et al., 2023), which integrates graph structures into imitation learning to skip redundant subgoal actions, and **BEAG** (Yoon et al., 2024), which uses breadth exploration with imaginary landmarks for goal-reaching. SSE is evaluated with the best

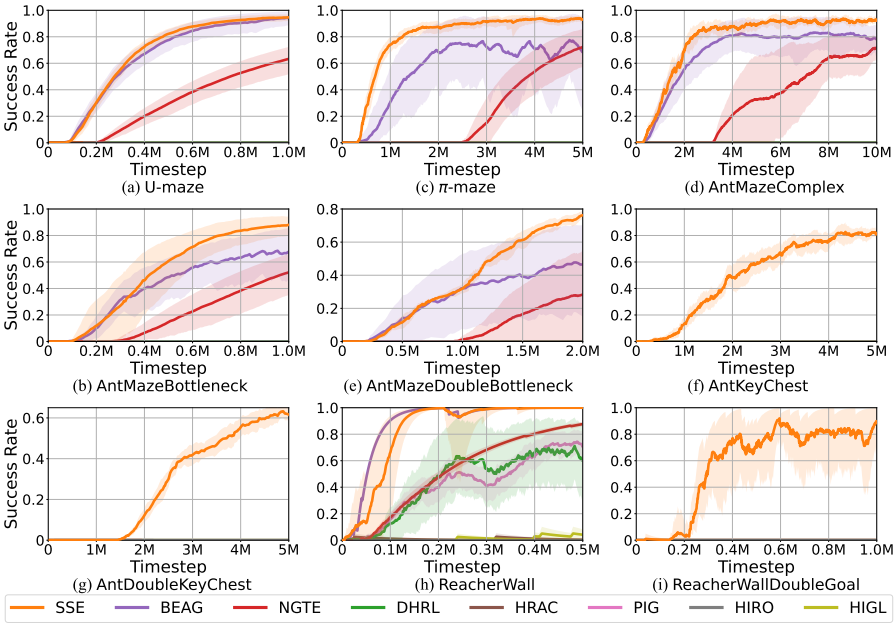

Figure 6: Performance comparison on various long-horizon environments

hyperparameter settings (c_{dist}, $d_{\mathcal{G}}$, η) from ablation studies, while all baselines use author-provided implementations. Detailed descriptions of each algorithm, along with the hyperparameter configurations for our proposed method, are provided in Appendix C.

Fig. 6 shows mean success rates over 5 seeds (solid lines) with standard deviations (shaded). SSE consistently outperforms both graph-based and conventional HRL methods across all benchmarks. Conventional HRL methods (DHRL, HIRO, PIG, HRAC, and HIGL) rely on random goal sampling for exploration but often struggle with fixed-goal tasks, while occasionally succeeding in random-goal setups provided in Appendix D.1, highlighting the increased challenge of fixed goals due to limited exploration opportunities. In relatively simple environments such as `U-maze`, `π-maze`, and `AntMazeComplex`, baseline methods like BEAG and NGTE demonstrate reasonable performance, but SSE typically converges more quickly. In bottleneck environments, SSE further excels by using failure-aware path refinement to avoid unstable regions as shown in Fig. 3. In more complex tasks like KeyChest and `ReacherWallDoubleGoal`, which require reaching intermediate objectives, baseline methods largely fail. Conventional HRL suffers from long high-level horizons, and goal-centric methods without high-level decision-making, such as BEAG, cannot reason about intermediate targets. In contrast, SSE mitigates these issues by strictly enforcing subgoal completion, reducing high-level decision steps. These results highlight the versatility, efficiency, and generalization of the proposed SSE framework. For practical comparison, we also evaluate the computational complexity against major baselines in Appendix D.2. The results show that our method achieves lower complexity per iteration, demonstrating its superiority in terms of computational efficiency.

5.2 Further Analysis and Ablation Studies

Fig. 7 presents a trajectory analysis of the proposed SSE framework in the `AntDoubleKeyChest` environment, illustrating how the agent progressively explores the map and collects both keys and the final goal. In the early stage (a) ($t \approx 300$K), the agent expands map coverage by sampling diverse subgoals, similar to simpler environments. As training progresses, the agent visits increasingly more regions, allowing it to reach the first key within a single high-level step, as shown in (b) ($t \approx 1$M). In a more advanced stage (c) ($t \approx 1.5$M), it collects both keys in just two high-level steps. Eventually, as shown in (d) ($t \approx 3$M), the agent completes the entire task, including both keys and the goal, in only three high-level steps. These results demonstrate that SSE allows the agent to reach any location in the map with a single high-level decision. As a result, it can solve complex multi-goal tasks using a minimal number of high-level steps, which highlights the effectiveness of SSE in long-horizon environments that require sequential decision-making for the high-level policy. Notably, SSE solves this sequential task without an explicit curriculum. The reliability of its high-level policy, learned via FER, combined with an augmented state including key-possession flags, enables the agent to autonomously discover the required sequence of sub-objectives.

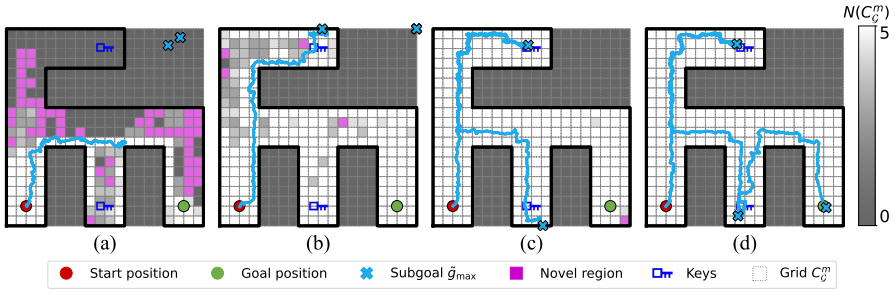

Figure 7: Trajectory analysis for SSE subgoals $\tilde{g}_{\max}$ in `AntDoubleKeyChest` at: (a) early stage, (b) reaches first key, (c) collects both keys, (d) reaches goal after collecting both keys (task success).

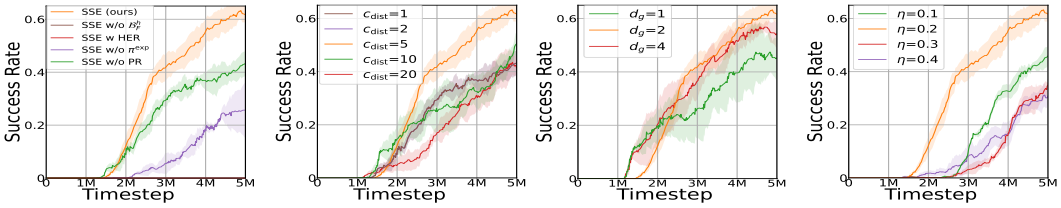

(a) Component evaluation (b) Distance scaling c_{dist} (c) Grid size $d_{\mathcal{G}}$ (d) Exploration ratio η

Figure 8: Ablation study on `AntDoubleKeyChest` environment

We conduct an ablation study on `AntDoubleKeyChest` to evaluate the contribution of each component in SSE and to analyze the impact of key hyperparameters, as shown in Fig. 8. For the component analysis, we consider four variants: (1) **SSE without** $\mathcal{B}_F^h$, which disables FER by using a standard replay buffer; (2) **SSE with HER**, which replaces strict subgoal execution with a conventional high-level policy that uses HER; (3) **SSE without** π^{exp}, which disables the exploration policy; and (4) **SSE without path refinement (PR)**, which disables the failure-aware adjustment. All variants exhibit degraded performance. Notably, the settings using HER or disabling FER fail to learn entirely, emphasizing the importance of strict subgoal execution and the consistent high-level signals provided by FER. Our hyperparameter analysis shows that setting $c_{\text{dist}} = 5$ achieves an optimal balance, though performance holds steady across a range of values. Similarly, performance also holds steady for grid resolution, though overly fine grids (e.g., $d_{\mathcal{G}} = 1$) can slow learning. For the exploration ratio η, a value of 0.2 proves optimal. While hyperparameter tuning optimizes performance, SSE consistently outperforms all baselines. Additional analyses in other environments are presented in Appendix E, further validating these findings.

6 Limitation

Our framework introduces new hyperparameters, such as the exploration ratio η and path refinement factor c_{dist}, which require tuning. However, we find their effective ranges to be stable across diverse environments, and our ablation studies confirm that the framework maintains strong performance across a wide range of values, minimizing the overall tuning cost. While SSE also adds computational steps, its principle of early termination on subgoal failure yields significant efficiency gains. This prevents long, unproductive trajectories and results in a faster computation time compared to other recent methods, as quantitatively analyzed in Appendix D.2.

7 Conclusion

In this paper, We proposed SSE, a graph-based HRL framework designed to improve reliability and efficiency in long-horizon, goal-conditioned tasks. By enforcing single-step subgoal reachability, SSE enables more direct and reliable high-level planning and significantly reduces decision horizons. The introduction of failure-aware path refinement and a decoupled exploration policy further enhances subgoal reliability and map coverage. Extensive experiments demonstrate that SSE consistently outperforms existing HRL and graph-based methods across a range of complex tasks. These results highlight the framework's effectiveness in enabling stable and generalizable behavior, making it a promising approach for scalable hierarchical control in various long-horizon tasks.

ETHICS STATEMENT

This paper introduces a foundational algorithm, Strict Subgoal Execution (SSE), designed to improve the long-horizon planning capabilities of reinforcement learning agents. All experiments were conducted in standard, simulated robotics environments. As such, our research does not involve human subjects, sensitive or personally identifiable data, nor does it directly address systems that interact with people. Therefore, issues of data privacy, dataset bias, and fairness are not directly applicable to this work.

REPRODUCIBILITY STATEMENT

We are committed to the reproducibility of our research. The complete source code for our proposed framework, Strict Subgoal Execution (SSE), and all experiments is included as an anonymized zip file in the supplementary materials. A detailed breakdown of the implementation, including network architectures and training procedures, can be found in Appendix B. All hyperparameters required to reproduce our results are provided in Appendix C.3, with common settings listed in Table 2 and environment-specific configurations in Table 3. Furthermore, Appendix C details the full experimental setup, including descriptions of the baseline algorithms, specifications for all environments (Table 1), and the hardware and software configurations on which the experiments were conducted. We believe these resources will enable the reproduction of our findings.

REFERENCES

Marcin Andrychowicz, Filip Wolski, Alex Ray, Jonas Schneider, Rachel Fong, Peter Welinder, Bob McGrew, Josh Tobin, OpenAI Pieter Abbeel, and Wojciech Zaremba. Hindsight experience replay. *Advances in neural information processing systems*, 30, 2017.

Pierre-Luc Bacon, Jean Harb, and Doina Precup. The option-critic architecture. In *Proceedings of the AAAI conference on artificial intelligence*, volume 31, 2017.

Andrew G Barto and Sridhar Mahadevan. Recent advances in hierarchical reinforcement learning. *Discrete event dynamic systems*, 13:341–379, 2003.

Elliot Chane-Sane, Cordelia Schmid, and Ivan Laptev. Goal-conditioned reinforcement learning with imagined subgoals. In *International conference on machine learning*, pp. 1430–1440. PMLR, 2021.

Cédric Colas, Tristan Karch, Olivier Sigaud, and Pierre-Yves Oudeyer. Autotelic agents with intrinsically motivated goal-conditioned reinforcement learning: a short survey. *Journal of Artificial Intelligence Research*, 74:1159–1199, 2022.

Edsger W Dijkstra. A note on two problems in connexion with graphs. *Numerische mathematik*, 1 (1):269–271, 1959.

Adrien Ecoffet, Joost Huizinga, Joel Lehman, Kenneth O Stanley, and Jeff Clune. First return, then explore. *Nature*, 590(7847):580–586, 2021.

Ben Eysenbach, Russ R Salakhutdinov, and Sergey Levine. Search on the replay buffer: Bridging planning and reinforcement learning. *Advances in neural information processing systems*, 32, 2019.

Meng Fang, Tianyi Zhou, Yali Du, Lei Han, and Zhengyou Zhang. Curriculum-guided hindsight experience replay. *Advances in neural information processing systems*, 32, 2019.

Scott Fujimoto, Herke Hoof, and David Meger. Addressing function approximation error in actor-critic methods. In *International conference on machine learning*, pp. 1587–1596. PMLR, 2018.

Zhiao Huang, Fangchen Liu, and Hao Su. Mapping state space using landmarks for universal goal reaching. *Advances in Neural Information Processing Systems*, 32, 2019.

Matthias Hutsebaut-Buysse, Kevin Mets, and Steven Latré. Hierarchical reinforcement learning: A survey and open research challenges. *Machine Learning and Knowledge Extraction*, 4(1):172–221, 2022.

Leslie Pack Kaelbling. Learning to achieve goals. In *IJCAI*, volume 2, pp. 1094–1098. Citeseer, 1993.

Junsu Kim, Younggyo Seo, and Jinwoo Shin. Landmark-guided subgoal generation in hierarchical reinforcement learning. *Advances in neural information processing systems*, 34:28336–28349, 2021.

Junsu Kim, Younggyo Seo, Sungsoo Ahn, Kyunghwan Son, and Jinwoo Shin. Imitating graph-based planning with goal-conditioned policies. *arXiv preprint arXiv:2303.11166*, 2023.

Diederik P Kingma. Adam: A method for stochastic optimization. *arXiv preprint arXiv:1412.6980*, 2014.

Tejas D Kulkarni, Karthik Narasimhan, Ardavan Saeedi, and Josh Tenenbaum. Hierarchical deep reinforcement learning: Integrating temporal abstraction and intrinsic motivation. *Advances in neural information processing systems*, 29, 2016.

Seungjae Lee, Jigang Kim, Inkyu Jang, and H Jin Kim. Dhrl: a graph-based approach for long-horizon and sparse hierarchical reinforcement learning. *Advances in Neural Information Processing Systems*, 35:13668–13678, 2022.

Seungjae Lee, Daesol Cho, Jonghae Park, and H Jin Kim. Cqm: Curriculum reinforcement learning with a quantized world model. *Advances in Neural Information Processing Systems*, 36:78824–78845, 2023.

Andrew Levy, George Konidaris, Robert Platt, and Kate Saenko. Learning multi-level hierarchies with hindsight. *arXiv preprint arXiv:1712.00948*, 2017.

Minghuan Liu, Menghui Zhu, and Weinan Zhang. Goal-conditioned reinforcement learning: Problems and solutions. *arXiv preprint arXiv:2201.08299*, 2022.

Russell Mendonca, Oleh Rybkin, Kostas Daniilidis, Danijar Hafner, and Deepak Pathak. Discovering and achieving goals via world models. *Advances in Neural Information Processing Systems*, 34:24379–24391, 2021.

Volodymyr Mnih, Koray Kavukcuoglu, David Silver, Alex Graves, Ioannis Antonoglou, Daan Wierstra, and Martin Riedmiller. Playing atari with deep reinforcement learning. *arXiv preprint arXiv:1312.5602*, 2013.

Ofir Nachum, Shixiang Gu, Honglak Lee, and Sergey Levine. Near-optimal representation learning for hierarchical reinforcement learning. *arXiv preprint arXiv:1810.01257*, 2018a.

Ofir Nachum, Shixiang Shane Gu, Honglak Lee, and Sergey Levine. Data-efficient hierarchical reinforcement learning. *Advances in neural information processing systems*, 31, 2018b.

Ofir Nachum, Haoran Tang, Xingyu Lu, Shixiang Gu, Honglak Lee, and Sergey Levine. Why does hierarchy (sometimes) work so well in reinforcement learning? *arXiv preprint arXiv:1909.10618*, 2019.

Soroush Nasiriany, Vitchyr Pong, Steven Lin, and Sergey Levine. Planning with goal-conditioned policies. *Advances in neural information processing systems*, 32, 2019.

Jongchan Park, Seungjun Oh, and Yusung Kim. Novelty-aware graph traversal and expansion for hierarchical reinforcement learning. In *Proceedings of the 33rd ACM International Conference on Information and Knowledge Management*, pp. 1846–1855, 2024.

Shubham Pateria, Budhitama Subagdja, Ah-hwee Tan, and Chai Quek. Hierarchical reinforcement learning: A comprehensive survey. *ACM Computing Surveys (CSUR)*, 54(5):1–35, 2021.

Vitchyr H Pong, Murtaza Dalal, Steven Lin, Ashvin Nair, Shikhar Bahl, and Sergey Levine. Skew-fit: State-covering self-supervised reinforcement learning. *arXiv preprint arXiv:1903.03698*, 2019.

Tom Schaul, Daniel Horgan, Karol Gregor, and David Silver. Universal value function approximators. In *International conference on machine learning*, pp. 1312–1320. PMLR, 2015.

David Silver, Aja Huang, Chris J Maddison, Arthur Guez, Laurent Sifre, George Van Den Driessche, Julian Schrittwieser, Ioannis Antonoglou, Veda Panneershelvam, Marc Lanctot, et al. Mastering the game of go with deep neural networks and tree search. *nature*, 529(7587):484–489, 2016.

Emanuel Todorov, Tom Erez, and Yuval Tassa. Mujoco: A physics engine for model-based control. In *2012 IEEE/RSJ international conference on intelligent robots and systems*, pp. 5026–5033. IEEE, 2012.

Alexander Sasha Vezhnevets, Simon Osindero, Tom Schaul, Nicolas Heess, Max Jaderberg, David Silver, and Koray Kavukcuoglu. Feudal networks for hierarchical reinforcement learning. In *International conference on machine learning*, pp. 3540–3549. PMLR, 2017.

David Warde-Farley, Tom Van de Wiele, Tejas Kulkarni, Catalin Ionescu, Steven Hansen, and Volodymyr Mnih. Unsupervised control through non-parametric discriminative rewards. *arXiv preprint arXiv:1811.11359*, 2018.

Youngsik Yoon, Gangbok Lee, Sungsoo Ahn, and Jungseul Ok. Breadth-first exploration on adaptive grid for reinforcement learning. In *Forty-first International Conference on Machine Learning*, 2024.

Hongliang Zeng, Ping Zhang, Fang Li, Chubin Lin, and Junkang Zhou. Ahegc: Adaptive hindsight experience replay with goal-amended curiosity module for robot control. *IEEE Transactions on Neural Networks and Learning Systems*, 2023.

Amy Zhang, Sainbayar Sukhbaatar, Adam Lerer, Arthur Szlam, and Rob Fergus. Composable planning with attributes. In *International Conference on Machine Learning*, pp. 5842–5851. Pmlr, 2018.

Lunjun Zhang, Ge Yang, and Bradly C Stadie. World model as a graph: Learning latent landmarks for planning. In *International conference on machine learning*, pp. 12611–12620. PMLR, 2021.

Tianren Zhang, Shangqi Guo, Tian Tan, Xiaolin Hu, and Feng Chen. Generating adjacency-constrained subgoals in hierarchical reinforcement learning. *Advances in neural information processing systems*, 33:21579–21590, 2020.

A THE USE OF LARGE LANGUAGE MODELS

We utilized a large language model (LLM) as an assistive tool during the preparation of this manuscript. The LLM's role was strictly limited to polishing the text, which includes improving clarity, conciseness, and correcting grammatical errors. The LLM was not used for research ideation. The authors have carefully reviewed and edited all content and take full responsibility for the scientific accuracy and integrity of this work. The LLM is not credited as an author.

B IMPLEMENTATION DETAILS

This section presents additional implementation details of the proposed SSE framework. The graph construction method for the proposed SSE is detailed in Appendix B.1, while the training dynamics and implementation specifics of the framework are described in Appendix B.2. Each subsection highlights the design motivations and practical considerations for each module or mechanism.

B.1 GRAPH CONSTRUCTION OF SSE

In this section, we describe how existing methods define the graph $G = (V, E)$,which consists of a landmark node set V and the edge set E with edge distances d. We then explain how the proposed SSE framework constructs this graph.

Landmark Node Set V Construction

Existing HRL methods such as DHRL (Lee et al., 2022) and NGTE (Park et al., 2024) construct the landmark node set V by selecting visited states during exploration. They employ the Farthest Point Sampling (FPS) algorithm to identify landmark nodes that are far apart from each other. This approach ensures that frequently visited regions are well-represented, as it builds V based on actual agent trajectories. However, it is limited to visited states, meaning unexplored or infrequently visited areas cannot be selected as landmarks, slowing exploration in those regions. In contrast, BEAG (Yoon et al., 2024) accelerates exploration by partitioning the goal space into a grid structure, creating landmark nodes at each grid intersection. This method allows for faster exploration by using virtual goal positions as landmarks, independent of visitation frequency. The structured grid layout enables more systematic and efficient exploration. To leverage this advantage and ensure a structured, reproducible setup, SSE adopts a grid-based landmark selection strategy inspired by BEAG. Given a 2D goal space of size $x \times y$ and a grid size of $d_{\mathcal{G}}$, the landmark set V is constructed as follows:

$$V = \{(i \cdot d_{\mathcal{G}}, j \cdot d_{\mathcal{G}}) \in \mathcal{G} \mid i = 0, \cdots, \frac{x}{d_{\mathcal{G}}} - 1,\ j = 0, \cdots, \frac{y}{d_{\mathcal{G}}} - 1\}. \tag{6}$$

For a 3D goal space, the landmark node set is defined as $V = \{(i \cdot d_{\mathcal{G}}, j \cdot d_{\mathcal{G}}, k \cdot d_{\mathcal{G}}) \in \mathcal{G} \mid i = 0, \cdots, \frac{x}{d_{\mathcal{G}}} - 1,\ j = 0, \cdots, \frac{y}{d_{\mathcal{G}}} - 1,\ k = 0, \cdots, \frac{z}{d_{\mathcal{G}}} - 1\}$. By constructing landmark nodes in this grid-based manner, SSE achieves faster and more structured exploration compared to visitation-based methods, ensuring efficient path planning and reliable subgoal execution.

Definition of Edge Distance

Given the landmark node set V, the edge set E is defined as the collection of distances $d(v_1 \to v_2)$ between any two nodes $v_1, v_2 \in V$. For previous graph-based RL methods, the edge distance d is computed as $d(v_1 \to v_2) := \log_{\gamma^l}\left(1 + (1-\gamma^l)Q^G(v_1, v_2, \pi^l)\right)$, where γ^l is the low-level discount factor used for training the low-level policy π^l, and Q^G is the value function estimating the traversal cost from v_1 to v_2, as described in Section 2. Existing HRL methods like DHRL (Lee et al., 2022) and NGTE (Park et al., 2024) directly use the low-level value function Q^l, which is trained with a step-based reward of -1, to define the distance as the expected number of steps required for the low-level policy to navigate from v_1 to v_2. Although this method reflects actual navigation costs, it is sensitive to instability during Q^l training, resulting in fluctuating edge distances. In contrast, BEAG (Yoon et al., 2024) measures the distance using the Euclidean norm $d_E = ||v_1 - v_2||$, providing a stable but less accurate representation of traversal costs. To leverage the strengths of both approaches, SSE defines the edge distance $d(v_1 \to v_2)$ by combining Q^l and d_E as follows:

$$d(v_1 \to v_2) = \frac{1}{2}\left[\log_{\gamma^l}\left(1 + (1-\gamma^l)Q^l(v_1, v_2, \pi^l)\right) + \log_{\gamma^l}\left(1 + (1-\gamma^l)d_E(v_1, v_2)\right)\right]. \tag{7}$$

This hybrid formulation allows SSE to benefit from the stability of Euclidean distances when Q^l is not fully converged, while still capturing the true traversal cost as Q^l improves. As a result, the edge set E is constructed as $E = \{d(v_1 \to v_2) \mid v_1, v_2 \in V\}$. Here, d represents the raw edge distance before failure-aware path refinement is applied, ensuring both stability and adaptive accuracy in path estimation.

B.2 Detailed Loss Functions and Implementation of the SSE Framework

As described in Section 4, the proposed SSE framework is an HRL structure that employs a high-level policy π^h, an exploration policy π^{exp}, and a low-level policy π^l. The exploration policy does not require separate parameterization for high-level actions, whereas π^h and π^l are parameterized by θ^h and θ^l, respectively, and are represented as $\pi^h_{\theta^h}$ and $\pi^l_{\theta^l}$. To evaluate these policies, SSE defines the parameterized high-level value function $Q^h_{\psi^h}$ and the low-level value function $Q^l_{\psi^l}$, where ψ^h and ψ^l are the respective parameters. As mentioned in Section 2, the high-level policy and value function are trained to maximize external rewards, while the low-level policy and value function are optimized to reach designated waypoints incrementally. To facilitate this, the low-level policy receives the reward r^l_t at each time step, defined as follows:

$$r^l_t = \begin{cases} 0 & \text{if } \|\phi(s_{t+1}) - \text{wp}_i\| < 0.5, \text{ (agent reaches the current waypoint)} \\ -1 & \text{otherwise,} \end{cases} \tag{8}$$

where wp_i is the target waypoint at the current timestep t, and $(\text{wp}_1, \cdots, \text{wp}_n)$ represent the shortest path from $\phi(s_t)$ to the subgoal $\tilde{g}_t$. The high-level and low-level policies, along with their value functions, are trained using the transitions stored in the FER $\mathcal{B}^h_F$ and the low-level buffer $\mathcal{B}^l$ through the TD3 algorithm (Fujimoto et al., 2018), a standard off-policy RL method. The value function losses for high-level and low-level policies are defined as follows:

$$\begin{aligned} \mathcal{L}_{Q^h}(\psi^h) &= \mathbb{E}_{B^h_F}\left[\left(Q^h(s_t, \tilde{g}_t) - \left(r^h_t + \gamma^h \min_{i=1,2} Q^h_{\bar{\psi}^h_i}(s_{t'}, \pi^h_{\theta^h}(s_{t'}, g))\right)\right)^2\right] \\ \mathcal{L}_{Q^l}(\psi^l) &= \mathbb{E}_{B^l}\left[\left(Q^l(s_t, a_t) - \left(r^l_t + \gamma^l \min_{i=1,2} Q^l_{\bar{\psi}^l_i}(s_{t+1}, \pi^l_{\theta^l}(s_{t+1}, \text{wp}_i))\right)\right)^2\right], \end{aligned} \tag{9}$$

where t' denotes the termination time of the low-level path execution, which is variable as the step concludes only upon success or failure. In the case of a partial success, t_{wp} (used to store transitions in FER) indicates the time step when the agent reached the last successful waypoint wp_{final}. The high-level reward is then defined as $r^h_t = \sum_{j=t}^{t'-1} r_j$ for a successful trajectory and $r^h_t = 0$ for a failed one. The terms $\bar{\psi}^h$ and $\bar{\psi}^l$ are target network parameters updated via exponential moving average (EMA), and γ^h and γ^l are the discount factors for training the high-level and low-level policies, respectively. The actor losses for optimizing the policies are defined as follows:

$$\mathcal{L}_{\pi^h}(\theta^h) = -\mathbb{E}_{B^h_F}\left[Q^h_{\psi^h}(s_t, \pi^h_{\theta^h}(s_t, g))\right], \quad \mathcal{L}_{\pi^l}(\theta^l) = -\mathbb{E}_{B^l}\left[Q^l_{\psi^l}(s_t, \pi^l_{\theta^l}(s_t, \text{wp}_i))\right]. \tag{10}$$

The parameters are optimized using the Adam optimizer (Kingma, 2014) to minimize the respective loss functions. SSE distinguishes between the high-level discount factor γ^h and the low-level discount factor γ^l, setting $\gamma^l = 0.99$ as typical in RL, and $\gamma^h = 0.4$ to limit return propagation across high-level steps, encouraging shorter path optimization. In the initial stages of training, rewards are sparse. To address this, the FER $\mathcal{B}^h_F$ is divided evenly, with half storing successful trajectories and the other half storing trajectories with zero reward. This design improves learning signals from successful experiences. The exploration ratio, which controls the balance between the exploration policy and the high-level policy, starts at 1:0 and decays by 0.05 per iteration until it reaches η:$(1-\eta)$, as outlined in Section 4. This scheduling promotes exploration initially and shifts the focus to high-level learning as training progresses. If the low-level agent fails to reach the high-level subgoal $\tilde{g}_t$, the trajectory is marked as failed. In cases where the agent becomes stuck, such as flipping over or hitting obstacles, its position may remain unchanged for long periods. To improve sample efficiency, if no movement is detected for 500 steps, the trajectory is classified as failed and the episode is terminated. The complete SSE algorithm is provided in Algorithm 2.

Algorithm 2 Strict Subgoal Execution (SSE)

Input: Graph $G = (V, E)$, goal g, mapping function ϕ, threshold λ, exploration ratio η
Initialize: Policies π^h, π^{exp}, π^l, buffers B_F^h, B^l, grid cells $C_{\mathcal{G}}$
for each iteration **do**
  for each episode **do**
    Select the behavior policy: $\pi \leftarrow \pi^{\text{exp}}$ with probability η, otherwise $\pi \leftarrow \pi^h$;
    for each high-level selection step **do**
      Sample a subgoal $\tilde{g}_t \sim \pi(s_t, g)$
      Plan the waypoint path $\text{wp}_{1:n}$ from $\phi(s_t)$ to $\tilde{g}_t$ using Dijkstra's algorithm over G with $\tilde{d}$
      for $i = 1, \cdots, n$ **do**
        Roll out the low-level policy $\pi^l(s_t, \text{wp}_i)$ to reach the waypoint wp_i
        Store the $t' - t$ transitions $(s_t, \text{wp}_i, a_t, r_t, s_{t+1})$ into the low-level buffer $\mathcal{B}^l$
        Compute the reward sum: $r_t^h = \sum_{j=t}^{t'-1} r_j$
        Construct the FER:
        if $\|\phi(s_{t+1}) - \tilde{g}_t\| < \lambda$ **then**
          Success: Store the success transition $(s, g, \tilde{g}_t, r_{\text{sum}}, s_{t'})$ into FER B_F^h
        else
          Failure: Store the stop-on-failure transition $(s, g, \tilde{g}_t, 0, s_T)$ into FER B_F^h
          Store the partial success transition $(s, g, \text{wp}_{\text{final}}, \sum_{j=t}^{t_{\text{wp}}-1} r_j, s_{t_{\text{wp}}})$ into FER B_F^h
          $N_{\text{fail}}(C_{\mathcal{G}}^m) += 1$ for m s.t. $\phi(s_{t'}) \in C_{\mathcal{G}}^m$
          Terminate the episode
        end
      end
    end
    $N(C_{\mathcal{G}}^m) += 1$ for all visited cells $C_{\mathcal{G}}^m$
  end
  Update ψ^h, θ^h using samples from FER B_F^h to minimize $\mathcal{L}_{Q^h}(\psi^h), \mathcal{L}_{\pi^h}(\theta^h)$
  Update ψ^l, θ^l using samples from $\mathcal{B}^l$ to minimize $\mathcal{L}_{Q^l}(\psi^l), \mathcal{L}_{\pi^l}(\theta^l)$
end

C Experimental Setup

Our proposed framework is designed to be modular and general, enabling integration with a wide range of baseline methods. For comparison, we employ the official codebases provided by the original authors for HIRO, HRAC, HIGL, DHRL, NGTE, and BEAG. All baselines are run using the hyperparameters specified in their respective publications, and conducted on an NVIDIA RTX 3090 GPU with an Intel Xeon Gold 6348 CPU (Ubuntu 20.04). Appendix C.1 provides descriptions of the baseline algorithms along with links to their official code repositories. Appendix C.2 provides the specifications for the nine environments shown in Fig.9, including their action and observation spaces, goal configurations, and episode horizons. The SSE-specific hyperparameter configurations for each environment are summarized in AppendixC.3.

C.1 Details of Other Baselines

- **HIRO** (Nachum et al., 2018b) introduces a hierarchical architecture with relabeling of high-level transitions to account for changing low-level policies, thereby improving off-policy sample efficiency and stability. Open-source code of HIRO is available at https://github.com/watakandai/hiro_pytorch
- **HRAC** (Zhang et al., 2020) adds a learned adjacency constraint to ensure subgoal feasibility. It penalizes high-level selections that attempt transitions deemed unreachable within a limited horizon, thereby guiding the agent to learn feasible subgoal structures. Open-source code of HRAC is available at https://github.com/trzhang0116/HRAC
- **HIGL** (Kim et al., 2021) incorporates a coverage-driven and novelty-driven landmark selection strategy. It performs graph-based planning via shortest paths and uses adjacency rewards

to guide learning toward under-explored regions. Open-source code of HIGL is available at https://github.com/junsu-kim97/HIGL

- **DHRL** (Lee et al., 2022) constructs a goal graph using Farthest Point Sampling and learns high-level behavior by planning over the graph. It emphasizes temporal abstraction and long-horizon planning via graph traversal and Q-learning. Open-source code of DHRL is available at https://github.com/jayLEE0301/dhrl_official
- **BEAG** (Yoon et al., 2024) employs value-function-driven imaginary landmarks to facilitate exploration of unvisited areas. It estimates landmark distances from a learned value function without relying solely on previously visited states, enabling efficient generalization. Open-source code of BEAG is available at https://github.com/ml-postech/BEAG
- **NGTE** (Park et al., 2024) drives novelty-based exploration by identifying frontier nodes (outposts) and prioritizing expansion toward less-visited regions of the goal graph, encouraging broad and diverse exploration. Open-source code of NGTE is available at https://github.com/ihatebroccoli/NGTE

C.2 Environmental Details

We follow standard benchmarks and configurations widely adopted in prior hierarchical reinforcement learning studies (Lee et al., 2022; Park et al., 2024; Yoon et al., 2024), and introduce several new environments designed to evaluate high-level decision-making capabilities such as `AntKeyChest` or `AntDoubleKeyChest`. The environments used in our experiments are visualized in Fig. 9, and their characteristics are described in Table 1.

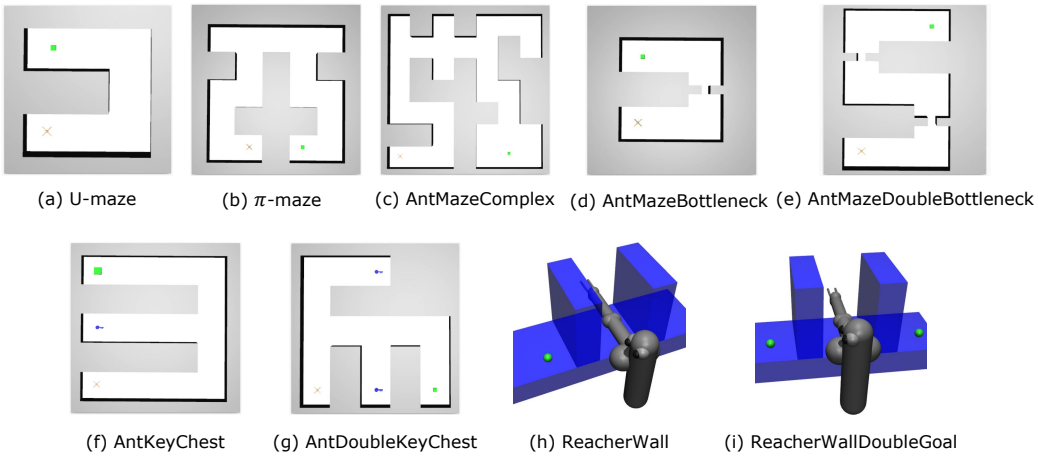

Figure 9: Considered long-horizon environments: 5 AntMaze, 2 KeyChest, and 2 Reacher tasks

`AntKeyChest` and `AntDoubleKeyChest` include key flags that are toggled from 0 to 1 when the agent successfully reaches the corresponding key location under a predefined condition. `ReacherWallDoubleGoal` contains two distinct goal positions, and two goal vectors are provided along with corresponding success flags, which are set to 1 upon reaching each goal. The success threshold for determining whether a target is reached is 5 in the AntMaze environments and 0.25 in the Reacher environments.

C.3 Hyperparameter Setup

Table 2 summarizes the common hyperparameters used across all environments. These configurations are based on a combination of parameter tuning and default settings from baseline implementations. In particular, the buffer size, batch size, and network architecture follow the original baseline code. Learning rates for each policy level, as well as the discount factors, were determined through a structured parameter search.

Table 3 presents environment-specific hyperparameters, including the minimum epsilon threshold ϵ_{min}, the path refinement scaling factor c_{dist}, the subgoal success threshold λ, and the grid resolution

Table 1: Summary of environment specifications.

Environment	Spaces (Obs / Action)	Goal space	Reward	Start / Goal Position	Episode length
`U-Maze`	Obs: 29-Dof Action: 8-Dof	[-4,20]× [-4,20]	1 if goal reached else 0	Start: (0,0) Goal: (0,16)	600
`π-Maze`	Obs: 29-Dof Action: 8-Dof	[-4,36]× [-4,36]	1 if goal reached else 0	Start: (8,0) Goal: (24,0)	1000
`AntMazeComplex`	Obs: 29-Dof Action: 8-Dof	[-4,52]× [-4,52]	1 if goal reached else 0	Start: (0,0) Goal: (40,0)	2000
`AntMazeBottleneck`	Obs: 29-Dof Action: 8-Dof	[-4,20]× [-4,20]	1 if goal reached else 0	Start: (0,0) Goal: (0,16)	600
`AntMazeDoubleBottleneck`	Obs: 29-Dof Action: 8-Dof	[-4,20]× [-4,36]	1 if goal reached else 0	Start: (0,0) Goal: (16,32)	1200
`AntKeyChest`	Obs: 30-Dof Action: 8-Dof	[-4,36]× [-4,36]	1 if key reached 5 if goal reached with key	Start: (0,0) Key: (0,16) Goal: (0,32)	2000
`AntDoubleKeyChest`	Obs: 31-Dof Action: 8-Dof	[-4,36]× [-4,36]	1 if key1 reached 1 if key2 reached with key1 5 if goal reached with two keys	Start: (0,0) Key1: (16, 32) Key2: (16, 0) Goal: (32, 0)	3000
`ReacherWall`	Obs: 17-Dof Action: 7-Dof	[-1,1]× [-1,1]× [-1,1]	1 if goal reached	Start: (0.99, −0.19, 0) Goal: (0.6, 0.6, −0.1)	100
`ReacherWallDoubleGoal`	Obs: 22-Dof Action: 7-Dof	[-1,1]× [-1,1]× [-1,1]	1 if goal reached 5 if both goals reached	Start: (0.99, −0.19, 0) Goal1: (0.4, 0.4, −0.1) Goal2: (0.4, −0.8, −0.1)	200

$d_{\mathcal{G}}$. These values were selected based on targeted parameter searches conducted for each environment.

In the case of `AntDoubleKeyChest`, a higher value of ϵ_{min} is required compared to other environments. This is because the task involves discovering multiple intermediate objectives, which increases the need for broad exploration. Other parameters such as the exploration ratio η and the refinement scaling factor c_{dist} were also selected through environment-specific tuning, with further analyses reported in Appendix E.2.

Table 2: Common hyperparameter settings used in SSE.

Hyperparameter	**Value**
Optimizer	Adam
Replay buffer size	2,500,000
Batch size	1024
High-level actor learning rate α^h_{actor}	0.000005
High-level critic learning rate α^h_{critic}	0.00005
Low-level actor learning rate α^l_{actor}	0.0001
Low-level critic learning rate α^l_{critic}	0.001
High-level discount factor γ^h	0.4
Low-level discount factor γ^l	0.99
Target update rate τ	0.005

Table 3: Scenario-specific hyperparameters for SSE.

Scenario	ϵ_{min}	c_{dist}	λ	$d_{\mathcal{G}}$	η
AntMaze					
`U-maze`	0.1	5.0	2.0	2	0.1
`AntMazeBottleneck`	0.1	5.0	2.0	2	0.1
`π-maze`	0.1	5.0	2.0	2	0.2
`AntMazeComplex`	0.1	5.0	2.0	2	0.2
`AntMazeDoubleBottleneck`	0.1	10.0	2.0	2	0.1
`AntKeyChest`	0.1	5.0	2.0	2	0.2
`AntDoubleKeyChest`	0.2	5.0	2.0	2	0.2
Reacher					
`ReacherWall`	0.1	5.0	0.15	1	0.2
`ReacherWallDoubleGoal`	0.1	5.0	0.15	1	0.2

D Additional Comparative Experiments

This section presents additional comparative experiments to further assess the generality and computational efficiency of the proposed SSE framework. We evaluate performance in a random-goal training setup in Appendix D.1, where goals are sampled uniformly from the entire reachable state space. Appendix D.2 evaluates computational characteristics, including convergence speed and per-episode compute time.

D.1 Performance Comparison under Random Goal Setups

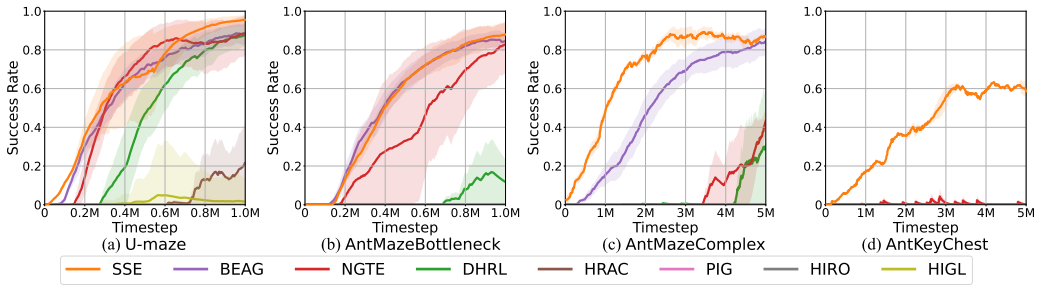

Figure 10: Performance comparison in random goal setting

In Fig. 10, we compare experimental results under a random goal setting, where the goal is sampled uniformly from the entire valid state space during training, unlike the fixed-goal scenarios discussed in the main text. The reward signal remains sparse, posing a significant challenge for goal discov-

ery and policy optimization. Graph-based methods such as BEAG, NGTE, and SSE, which can autonomously expand their subgoal graph during exploration, maintain strong performance even under random goal sampling, achieving success rates comparable to those in the fixed-goal setting. DHRL also benefits from the randomized goal distribution, particularly in simpler environments like `U-maze` and `AntMazeBottleneck`, where the training signal is more frequently encountered. On the other hand, methods such as HIRO, HIGL, and HRAC exhibit limited progress in most environments under random-goal conditions, due to their reliance on fixed-frequency subgoal selection, sparse reward setting, and lack of structured exploration mechanisms. In environments requiring multi-stage reasoning such as `AntKeyChest`, SSE is the only method that consistently discovers the key and solves the full task. NGTE, while hierarchical and exploration-driven, occasionally learns to acquire the key, but overall exhibits a very low success rate under this random goal configuration.

D.2 Computational Complexity Comparison

Table 4 reports the average per-episode computation time and the number of episodes required to reach a 60% success rate with NGTE and BEAG. We compare against NGTE and BEAG because they are the only baselines that succeed in at least one of the considered fixed-goal settings, making them the most relevant references for evaluating performance and sample efficiency in sparse reward environments. SSE achieves faster convergence across tasks due to its early termination of episodes upon subgoal failure and a reduced number of transitions per episode, which minimizes unnecessary computation and accelerates learning.

This advantage is particularly evident in long-horizon tasks such as `AntKeyChest`, where conventional HRL methods consume many timesteps even during failed attempts and require extended horizons for high-level planning. In contrast, in shorter-horizon scenarios such as `AntMazeBottleneck`, the computational benefits of SSE are less significant since subgoal transitions and failure terminations occur less frequently. The operations introduced by SSE, including the evaluation of subgoal completion and uniform sampling, are lightweight and have linear time complexity. As a result, SSE imposes minimal computational overhead while maintaining stable training dynamics.

Table 4: Average per-episode computation time (in seconds) and the number of episodes required to reach 60% success rate.

Scenario	**SSE**	**BEAG**	**NGTE**
`AntMazeBottleneck`	5.94s 432 episodes	6.46s 425.2 episodes	12.65s 725.6 episodes
`AntKeyChest`	18.13s 1658 episodes	57.29s fail	119.07s fail

E Extended Analyses of the Proposed SSE Framework

To further validate the design and generality of SSE, this section presents extended analyses across several dimensions. Appendix E.1 provides qualitative trajectory visualizations that illustrate how SSE dynamically adapts its subgoal planning over time. Appendix E.2 presents ablation and sensitivity analyses to isolate the contribution of individual components and hyperparameters, including the path refinement scale c_{dist}, grid resolution $d_{\mathcal{G}}$, and exploration ratio η.

E.1 Trajectory Analysis in Other Environments

To gain deeper insight into the behavior of SSE, we present trajectory analyses across representative environments.

Fig. 11 illustrates learning progression in `AntMazeBottleneck`. In the early stage (a), the agent has not yet discovered feasible subgoals, causing the high-level policy π^h selects subgoals largely at random. During this phase, the exploration policy promotes coverage by gradually expanding

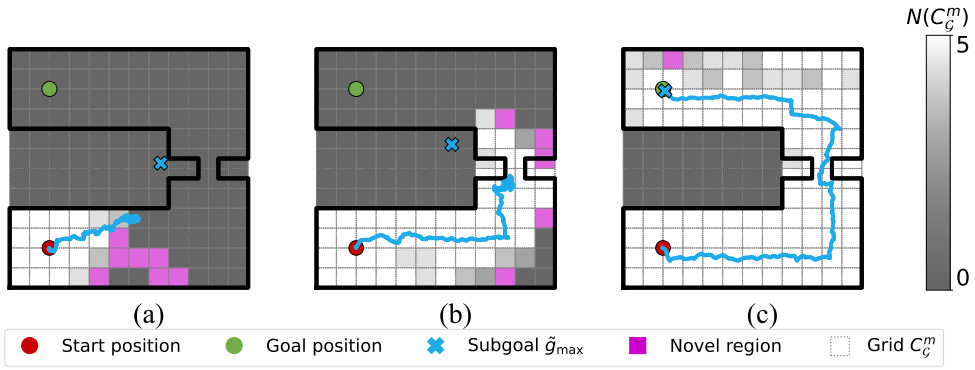

Figure 11: Trajectory analysis of SSE subgoals $\tilde{g}_{\max}$ in `AntMazeBottleneck` across: (a) early stage, (b) mid training, and (c) task success.

into novel regions. In the mid stage (b), the agent fails to traverse the narrow bottleneck, primarily because the low-level policy π^l lacks sufficient experience in that region and the associated failure statistics $\text{ratio}_{\text{fail}}$ remain underrepresented. By the final stage (c), SSE successfully leverages failure-aware refinement and subgoal selection, allowing π^h to navigate through the bottleneck and reach the goal reliably.

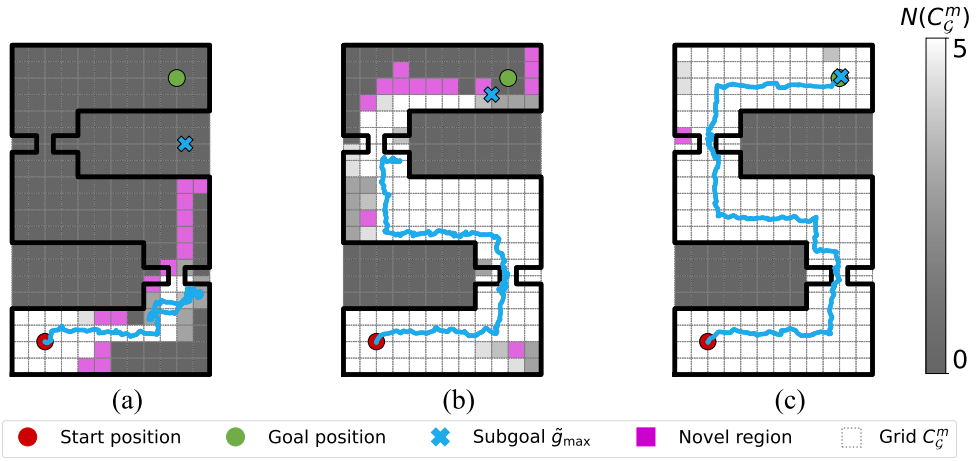

Figure 12: Trajectory analysis of SSE subgoals $\tilde{g}_{\max}$ in `AntMazeDoubleBottleneck` across: (a) early stage, (b) mid training, and (c) task success.

A similar trend is observed in `AntMazeDoubleBottleneck` as Fig. 12. Initially (a), most regions are unexplored, and subgoal selection remains uninformed. In the intermediate phase (b), the agent again struggles with the second bottleneck due to insufficient failure feedback. As training progresses (c), subgoals selected by π^h become more effective, and the updated path refinement guides the agent through safer routes, enabling successful traversal of both bottlenecks and completion of the long-horizon task.

In Fig. 13, the agent in `AntKeyChest` begins by exploring the environment without a clear objective (a). Upon discovering the key (b), π^h increasingly selects subgoals leading to the key location. In the final stage (c), the agent demonstrates the ability to sequentially reason over subtasks, first reaching the key and then navigating to the final goal with the required flag active, completing the task successfully.

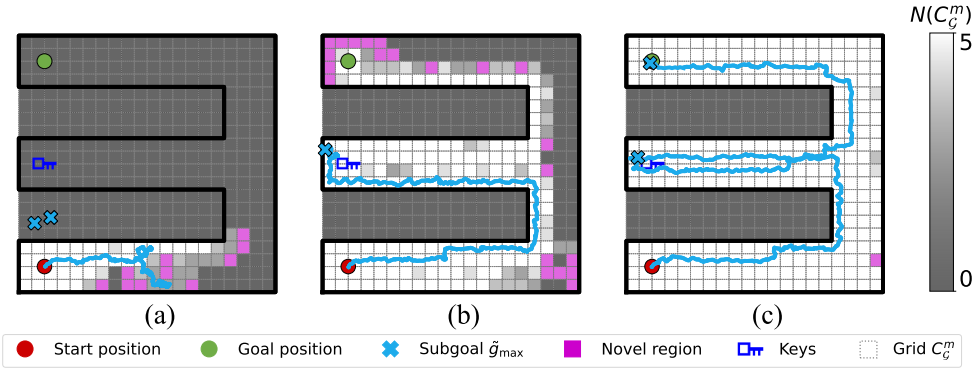

Figure 13: Trajectory analysis of SSE subgoals $\tilde{g}_{\max}$ in `AntKeyChest` across: (a) early stage, (b) after reaching the key, and (c) reaching the goal with the key (task success).

E.2 Additional Ablation Studies

Component Evaluation

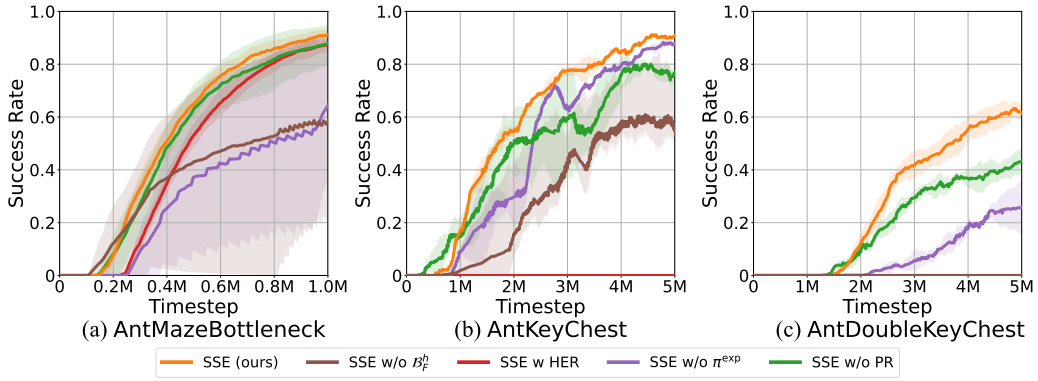

Figure 14: Component evaluation results in various maps

Fig. 14 presents the performance of SSE variants with key components ablated. Specifically, we evaluate four variants: (1) a version that disables FER by replacing its buffer with a conventional replay buffer (SSE w/o $\mathcal{B}_F^h$); (2) a version that replaces our strict execution with a conventional fixed-step HRL policy that uses HER (SSE with HER); (3) SSE without the decoupled exploration policy (SSE w/o π^{exp}); and (4) SSE without path refinement (SSE w/o PR). The results highlight the importance of each component. Removing path refinement (w/o PR) degrades performance, particularly in long-horizon settings where mitigating unreliable transitions is crucial. Disabling the exploration policy (w/o π^{exp}) consistently harms performance across all environments, confirming the importance of structured exploration for goal-space coverage. Finally, the variants that alter the core learning signal, SSE with HER and SSE w/o $\mathcal{B}_F^h$, exhibit a similar pattern. Both manage to achieve some success in the simpler `AntMazeBottleneck` environment but largely fail to solve complex, multi-stage tasks like `AntDoubleKeyChest`. The failure of the HER variant shows that conventional hindsight relabeling provides an insufficient signal for subgoal feasibility. Likewise, disabling FER removes the **partial-success** and **stop-on-failure** transitions, which are critical for teaching the high-level policy to avoid unreliable subgoals. Together, these results underscore that our strict execution approach, through all its components, provides the clear and decisive signals necessary for effective long-horizon planning.

Effect of Path Refinement Scaling Factor c_{dist}

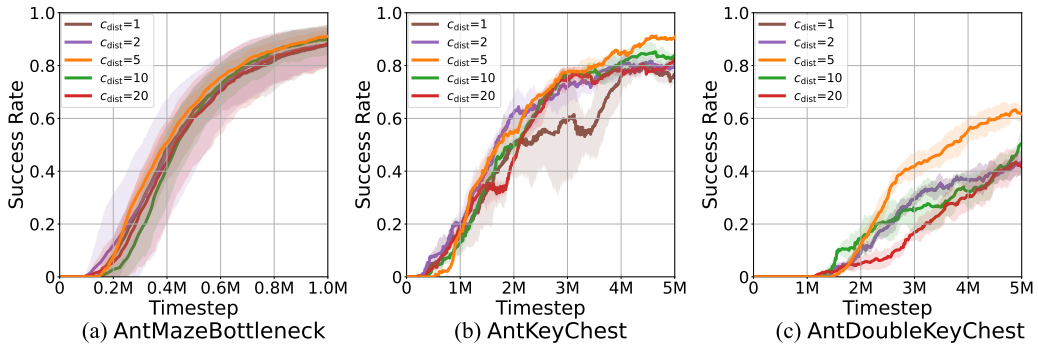

Figure 15: Distance scail c_{dist} analysis in various maps

Fig. 15 shows how the scaling factor c_{dist} affects performance. This parameter controls the trade-off between path efficiency and safety. In simpler tasks like `AntMazeBottleneck`, its impact is minimal. In more complex, long-horizon tasks, its role becomes more pronounced. A moderate value, such as $c_{\text{dist}} = 5$, provides an effective balance, guiding the planner away from failure-prone regions without being overly conservative. In contrast, excessively high values (e.g., 10 or 20) can lead to inefficient detours, while a value of 1 may not sufficiently penalize risky paths. Overall, the performance remains high for values between 2 and 10, indicating a wide effective range.

Effect of Grid Size $d_{\mathcal{G}}$

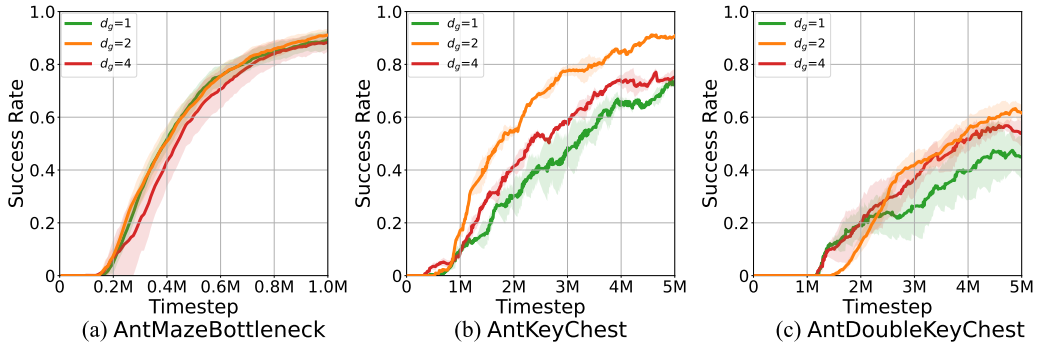

Figure 16: Grid size $d_{\mathcal{G}}$ analysis in various maps

Fig. 16 illustrates the effect of grid resolution $d_{\mathcal{G}}$. This parameter balances the granularity of novelty detection with the stability of failure statistics. The analysis shows that performance is not highly sensitive to this parameter within the tested range. For instance, in AntMaze environments, there is little significant difference in performance for $d_{\mathcal{G}}$ values of 1, 2, and 4. A coarse grid ($d_{\mathcal{G}} = 4$) may merge distinct regions, while an overly fine grid ($d_{\mathcal{G}} = 1$) can make failure statistics less reliable. Thus, we find that a moderate resolution ($d_{\mathcal{G}} = 2$ for AntMaze) provides a suitable balance. The optimal choice is dependent on the environment's scale, with smaller, structured spaces like Reacher benefiting from a finer grid ($d_{\mathcal{G}} = 1$).

Effect of Exploration Ratio η

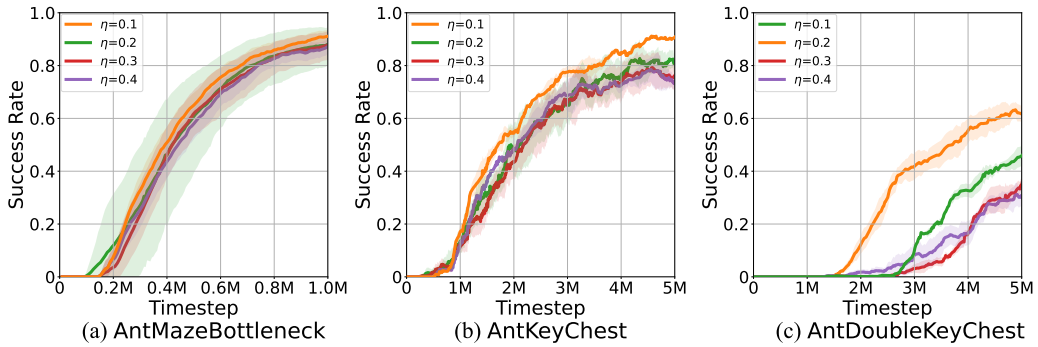

(a) AntMazeBottleneck (b) AntKeyChest (c) AntDoubleKeyChest

Figure 17: Exploration ratio η analysis in various maps

Fig. 17 shows how performance varies with the exploration ratio η, which controls the classic exploration-exploitation trade-off. In simple environments like `AntMazeBottleneck`, performance is consistent across a wide range of η values. In long-horizon tasks like `AntDoubleKeyChest` that require discovering intermediate objectives, the influence of η is naturally greater, but effective performance can be achieved with straightforward tuning. As shown in our experiments, setting the exploration ratio within a small range of 0.1 to 0.2 is sufficient to achieve strong performance across all tasks. This indicates that while the balance is important, extensive tuning of this hyperparameter is not required.